Extensive studies on the low-temperature properties of $TbPO_4$. III. Birefringence measurements and mean-field calculations

1993 J. Phys.: Condens. Matter 5 955

(http://iopscience.iop.org/0953-8984/5/7/023)

J. Phys.: Condens. Matter 5 (1993) 955–970. Printed in the UK

Extensive studies on the low-temperature properties of $TbPO_4$: III. Birefringence measurements and mean-field calculations

A U Müller†, J Jakelski‡ and H G Kahle
Physikalisches Institut, Universität Karlsruhe (TH), PO Box 6980, D–7500 Karlsruhe 1, Federal Republic of Germany

Received 18 June 1992, in final form 21 September 1992

Abstract. Measurements of the linear optical birefringence were used to determine the phase diagram of $TbPO_4$ at temperatures down to 1.4 K. At least one new structural and magnetic phase transition was found that is not detectable in magnetic investigations. Calculations using an appropriate mean-field Hamiltonian, including crystal distortions of monoclinic symmetry, allowed us not only to reproduce the experimental phase diagram very satisfactorily but also to give further insight into the magnetic structures and the distortions of the crystal in the various phases.

1. Introduction

Terbium phosphate has been studied extensively over the last two decades. Nevertheless, its physical low-temperature properties are still not clear in all details (see Mensinger *et al* 1993 for references). It crystallizes in the zircon structure with space group $I4_1/amd$ and site symmetry $\bar{4}m2$. In zero external field, it experiences two successive phase transitions (for details see the phase diagram of figure 5). The first one at $T_{N1} = 2.28$ K yields a simple two-sublattice antiferromagnet with the moments along the tetragonal c axis, indicated as AF till now or as AFc from now on. The second one at $T_{N2} = 2.13$ K leads to a canted antiferromagnet with the moments tilted off the c axis in a $\{110\}$ plane (still collinear) and the crystal symmetry is reduced to monoclinic by a cooperative Jahn–Teller effect; the phase is marked as AF′ till now or as AFxc/AFyc from now on. An external field along c produces first a spin-flop-like phase (SF) before the saturated paramagnetic phase (PM) is reached. Owing to the reduction of symmetry, the crystal is normally divided into crystallographic domains. Their distribution affects the observed properties of the material in a characteristic manner.

In the two preceding papers (Mensinger *et al* 1993, Anderer *et al* 1993, henceforth to be referred to as I and II, respectively), we presented studies of the magnetic properties and of the Faraday rotation on $TbPO_4$, including a general interpretation. In the present paper we report on renewed measurements of the linear optical birefringence on this substance that we have performed to complete a former

† Present address: Standard Elektrik Lorenz AG, D–7000 Stuttgart 40, Federal Republic of Germany.
‡ Present address: Höger, Stellrecht und Partner, Uhlandstr. 14c, D–7000 Stuttgart 1, Federal Republic of Germany.

0953-8984/93/070955+16$07.50

investigation (Becker *et al* 1985) and to elucidate the origin of small anomalies that were observed but had to remain unexplained. The recent findings, obtained with an improved experimental equipment, give clear evidence for additional phase transitions and hence for the existence of further magnetic and crystallographic phases. These phase transitions are obviously not detectable by magnetic measurements. As a consequence, the theoretical treatment that gave very acceptable results in the former investigations (Kasten and Üffinger 1985, Bluck and Kahle 1988) had to be modified and extended. We used a mean-field approach within the five-level system of the lowest Tb^{3+} states taking magnetic interactions and crystal distortions into account. This is described in section 4, and it is demonstrated that it leads to a very satisfactory agreement with the experimental findings. Some results of the present investigations have recently been published in a short communication (Kahle and Müller 1992).

2. Experimental details

Flux-grown crystals (Hintzmann and Müller-Vogt 1969) of different batches and with different dimensions were used. They were cut perpendicular to the tetragonal c axis and carefully polished with parallel surfaces. The deviation of the normals of these surfaces from the c direction was less than 30'. In this publication the findings on only one crystal will be shown and discussed in detail. Its dimensions and approximate demagnetizing factors are $a \times b \times c = 1.15 \times 1.6 \times 1.68$ mm^3, $N_a = 0.43$, $N_b = 0.29$, $N_c = 0.28$. Since the crystal is distorted below T_{N2}, its properties are described either in the system of the crystallographic a, b, c axes or in the system of the x, y, z axes, which are rotated by 45° around the $c \equiv z$ axis.

The crystal was placed in an exchange-gas cryostat with optical windows. It was irradiated with monochromatic light of different wavelengths λ parallel to the c axis. The birefringence was measured by using light modulation (50 kHz) and computer-controlled compensation of the corresponding phase difference by means of a Babinet–Soleil compensator. Details of the measuring procedure have been published elsewhere (Hess 1990). A resolution of 5×10^{-7} was obtained. Five different wavelengths were used: $\lambda = 632.8$ nm (He–Ne laser) and $\lambda = 436$, 547, 578 and 691 nm (mercury high-pressure lamp with interference filters of about 2.5 nm linewidth). The investigations were performed in the temperature region from 1.4 to 6.5 K and in magnetic fields up to 1.5 T, either at constant temperature as a function of field (field sweeps) or at constant field as a function of temperature (temperature sweeps). As a rule, the sweep velocity was 0.6 mT s^{-1} in the field sweeps and 1.25 mK s^{-1} in the temperature sweeps, respectively. Near to phase transitions the velocity was reduced by a factor of up to 4.

The quantities studied are the yx birefringence $\delta n_{yx} = n_y - n_x$ measured with the field along the x direction and the ba birefringence $\delta n_{ba} = n_b - n_a$ measured with the field along the a direction, respectively.

3. Experimental results

3.1. The yx birefringence

Figure 1 shows the field dependence of the yx birefringence measured in a special cycle of increasing and decreasing field strength at $T = 1.43$ K and $\lambda = 633$ nm. First the crystal was slowly cooled down in zero field. The birefringence is zero. In

increasing field along x (curve 1), at about 0.2 T the birefringence quickly rises to a value of 25×10^{-6}. Now the crystal is single-domain with regard to Γ_3^+, Γ_{5y}^+ distortions (AFyc phase, two-sublattice antiferromagnet, moments canted off the c axis in the yc plane, monoclinic crystal symmetry with x axis as monoclinic axis). Reversing the field-sweep direction at about 0.4 T (point 1/2), this phase remains stable even down to zero field (curve 2). Increasing the field anew (curve 3), the birefringence jumps exactly at the magnetic phase transition to the PMo phase (saturated paramagnet with orthorhombic symmetry, crystal is Γ_3^+ distorted) at $B_{C1}^x = 0.71$ T. In the following down sweep (curve 4), this phase transition shows a large hysteresis (of about 0.07 T) and a surprising hump ahead of the drop. Then the birefringence stays constant till around 0.2 T where it falls abruptly to a value of -25×10^{-6}. Now the crystal is single-domain in the AFxc phase, which has a Γ_3^+, Γ_{5x}^+ distortion orthogonal to that of the AFyc phase. The AFxc phase remains stable even at zero field. In the following up sweep (curve 5), the birefringence increases relatively steadily almost to the value of the AFyc phase and jumps again at the magnetic phase transition.

However, when the measuring cycle is carried out at a temperature above 1.58 K, the observed curves are quite different. Starting again with a slowly cooled crystal, the observed birefringence quickly falls from zero to a value of -25×10^{-6} at about 0.25 T. Now the crystal is single-domain in the AFxc phase and remains in this state even down to zero field. Increasing the field again, the birefringence stays almost constant at -25×10^{-6} till it makes a large jump to a positive value at the transition to the PMo phase (B_{C1}^x, temperature dependent). The subsequent down sweep shows hysteresis and the hump (as for $T = 1.43$ K); the drop afterwards though leads directly to the negative value of the AFxc phase.

These findings indicate that a magnetic field along x of sufficient strength induces an irreversible macroscopic Γ_3^+, Γ_5^+ distortion of the crystal as a whole. At $T = 1.43$ K, it is a distortion corresponding to the AFyc phase for a field of about 0.3 to 0.6 T and that corresponding to the AFxc phase for a field above 0.72 T. At a temperature above 1.58 K, however, it is always a distortion corresponding to the AFxc phase as soon as the field exceeds a value of about 0.3 T. These distortions are preserved at zero field. They even appear almost unchanged when the crystal was heated two or three times to 4.2 K and cooled again to the measuring temperature. Evidently, a memory of the former distortion must be stored in the crystal, for example, via a special strain distribution. This cannot be erased at 4.2 K, which means at a temperature above T_{N1} where the crystal is in the undistorted tetragonal phase. Warming the crystal to room temperature certainly eliminated the memory. If this 'tempered' crystal is cooled in zero field to a temperature below T_{N2} it will be Γ_3^+, Γ_5^+ distorted, but will be divided into domains of the phases AFyc and AFxc with roughly equal volume parts. Thus its birefringence will be almost zero. These were the starting conditions for the measurements described in figure 1.

The field dependence of the yx birefringence for different wavelengths is demonstrated in figure 2. Only sweeps with increasing field strength taken at 1.43 K are reproduced. Owing to preceding measurements the crystal in the main was in the AFxc phase at the beginning of each sweep. Here again the birefringence for a fixed wavelength has about the same size but different sign in the AFxc phase (in the range up to about 0.3 T) and in the AFyc phase (between about 0.4 and 0.7 T), respectively. But δn_{yx} changes sign between $\lambda = 547$ and 436 nm in the AFxc as well as in the AFyc phase. Above the magnetic phase transition at 0.71 T (PMo phase), on the contrary, the birefringence is strongly but steadily increasing with decreasing wavelength.

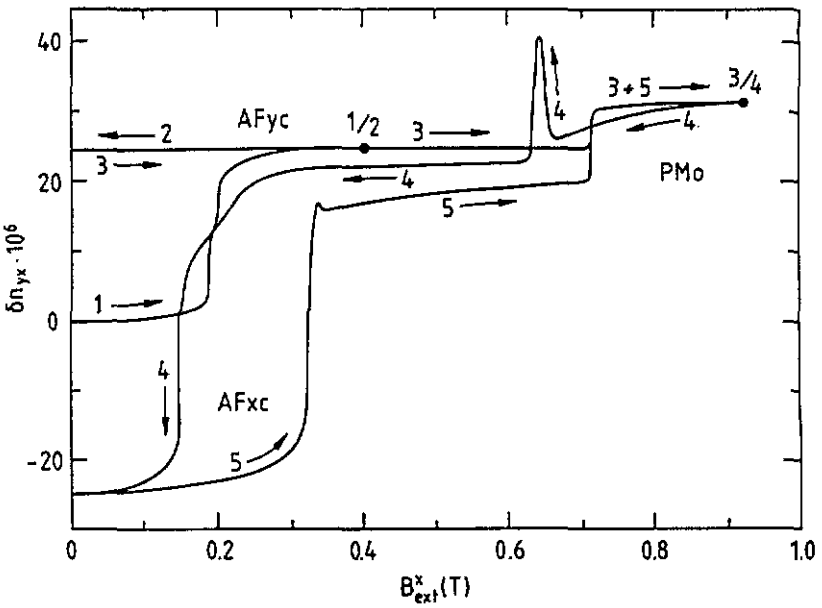

Figure 1. The yx birefringence measured for increasing and decreasing field along x at $T = 1.43$ K and $\lambda = 633$ nm. The numbers indicate the chronological sequence.

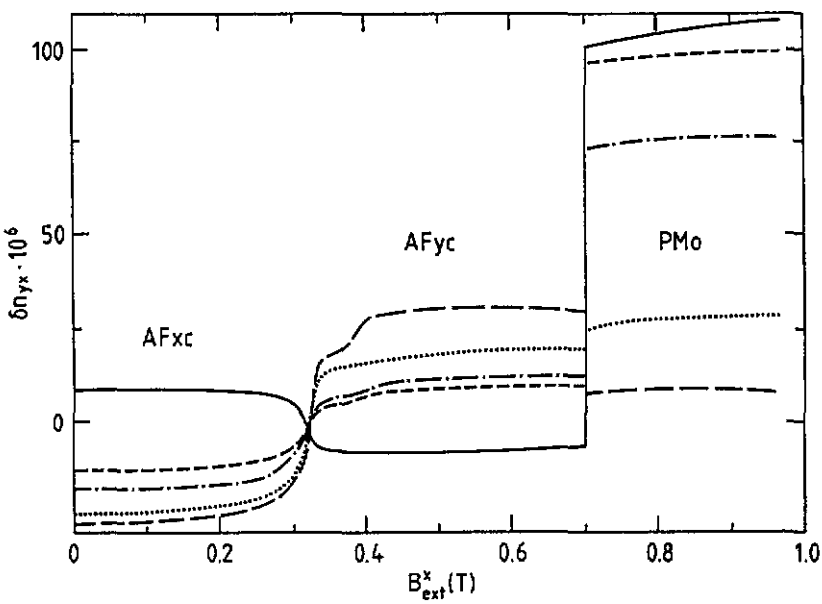

Figure 2. The yx birefringence measured at different wavelengths for increasing field along x at $T = 1.43$ K: full curve (scale reduced by a factor of 0.4), $\lambda = 436$ nm; short broken curve, $\lambda = 547$ nm; chain curve, $\lambda = 578$ nm; dotted curve, $\lambda = 633$ nm; long broken curve, $\lambda = 691$ nm.

In the down sweeps the magnetic phase transition is shifted to lower fields, as

mentioned already in connection with figure 1. This hysteresis is a strong indication that the Γ_3^+ distortion in the PMo phase is different from that in the AF*yc* phase. The calculations decribed in section 4 confirm this assumption. Accordingly the PMo and AF*xc* phases have the same direction of the Γ_3^+ distortion (with different sizes), but the AF*yc* phase the opposite one. Thus the sign of the birefringence measured at $\lambda = 436$ nm (in contrast to that measured at the other wavelengths) is directly correlated with the direction of the Γ_3^+ distortion.

In figure 3 the temperature dependence of the birefringence for different fields along x is reproduced for $\lambda = 436$ nm only. All curves show the same trend. They start at a small negative birefringence, indicating that the crystal is in a mixed state of AF*yc* and AF*xc* where AF*yc* is somewhat predominant. At the first increase the crystal becomes single-domain in the AF*xc* phase. The next drop (existing only till about 0.45 T) demonstrates the transition to the AF*c* phase (two-sublattice antiferromagnet, moments along c, tetragonal crystal symmetry) at T_{N2} and the following hump or jump that to the PMo phase at T_{N1}. At even higher temperatures the birefringence is decreasing, which means that the Γ_3^+ distortion is reduced with increasing temperature. The hysteresis between up and down sweeps is again striking, more or less distinct for all transitions independent of temperature and field strength.

3.2. The ba birefringence

Since the curves measured for the ba birefringence are even more puzzling than those of the yx birefringence, they will be discussed here only up to the point of determining the phase transitions. Some of the field sweeps are shown in figure 4. Curve 1, measured at $T = 1.42$ K and $\lambda = 633$ nm, is a simple curve; it starts at almost zero, steadily increases and drops down to a small negative value at the magnetic transition to the PMo phase at $B_{C1}^a = 0.87$ T. This tendency is maintained, in principle, at higher temperatures, again with different sign of δn_{ba} for $\lambda = 633$ and 436 nm up to B_{C1}^a, as found for δn_{yx}. For $T \geqslant 1.5$ K, however, in the up sweeps at $\lambda = 633$ nm (curves 3 and 4) and in the down sweeps at $\lambda = 436$ nm (curve 7) an additional jump or down-peak is to be seen somewhere below B_{C1}^a. The field values measured for these anomalies are linearly decreasing with increasing temperature (plotted as crosses in figure 7). These second jumps or peaks are serious indications of an intermediate phase lying in between the low-field antiferromagnetic (AF*xc*/AF*yx*) and the high-field paramagnetic (PMo) phase. No specification of this intermediate phase is possible from the size and the sign of the measured birefringence.

The temperature sweeps (not shown) reveal only the transition to the AF*c* phase for fields up to about 0.5 T. Above 0.9 T, δn_{ba} is small at all temperatures, but it shows an additional minute and broad anomaly, sometimes with a vague structure. The positions of the inflection point of the curves, measured in up or down sweeps or at different wavelengths, are spread over a certain range as indicated in figure 7 by the horizontal bars. Yet it seems possible to deduct an almost linear relation between field and temperature. Whether these anomalies actually represent phase transitions cannot be decided from experiment.

3.3. Phase diagram

Figures 5, 6 and 7 show the experimental phase diagram with fields along c, x and a, respectively. Demagnetization was taken into account only for the data reproduced in figure 5.

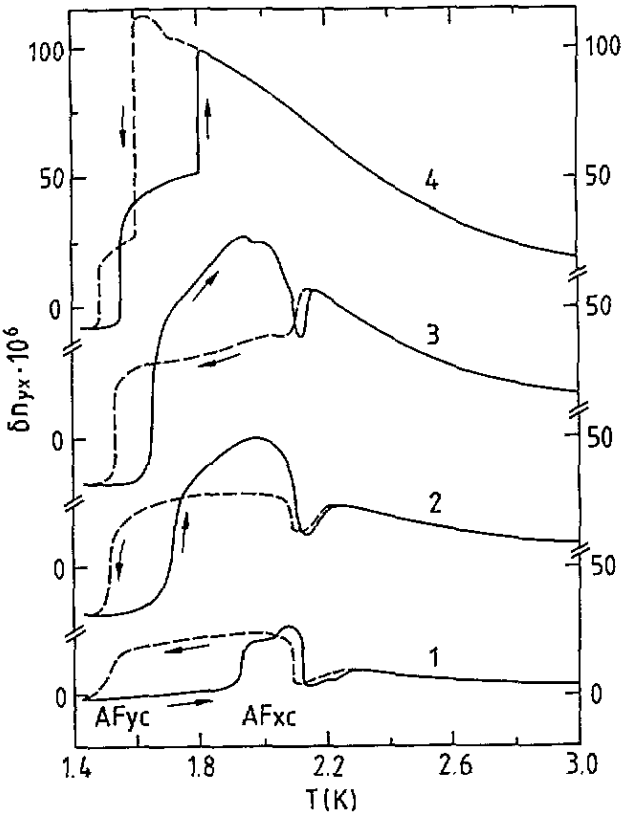

Figure 3. The yx birefringence measured at $\lambda = 436$ nm as a function of temperature for different field strengths along x, full curves for increasing, broken curves for decreasing temperature: 1, $B^x_{ext} = 0.2$ T; 2, $B^x_{ext} = 0.3$ T; 3, $B^x_{ext} = 0.4$ T; 4, $B^x_{ext} = 0.6$ T; scale reduced by a factor of 0.5.

In figure 5 the transition points obtained from the magnetization and magnetic susceptibility measurements of paper I are marked with open symbols, and those obtained from the Faraday rotation measurements of paper II with closed symbols. The full curves give the average of the points ascertained by Üffinger and Kasten (1985). The agreement is excellent in spite of the difficulties in the demagnetization procedure of the Faraday measurements (see paper II). The phase diagram with this field direction shows four phases: the paramagnetic phase PM; the plain antiferromagnetic phase AFc with moment direction along c and tetragonal symmetry; the antiferromagnetic phase AFxc or AFyc, which cannot be distinguished in this field direction, with the moments canted off the c axis and monoclinic symmetry (marked as AF' until now); and the spin-flop-like phase SF with orthorhombic symmetry. The structure of the two antiferromagnetic phases at zero external field are confirmed by neutron diffraction (Nägele *et al* 1980); the structure of the AFc phase also by magneto-electric effect (Rado *et al* 1984, Bluck and Kahle 1988). A study of the infrared transmission spectrum at zero field confirmed the monoclinic distortion of the crystal for temperatures below 2.12 K (Prinz and Lewis 1983). The transition temperatures at zero field, found in the present investigations, are consistent with our former results, $T_{N1} = 2.28 \pm 0.02$ K and $T_{N2} = 2.13 \pm 0.02$ K, and the bicritical point,

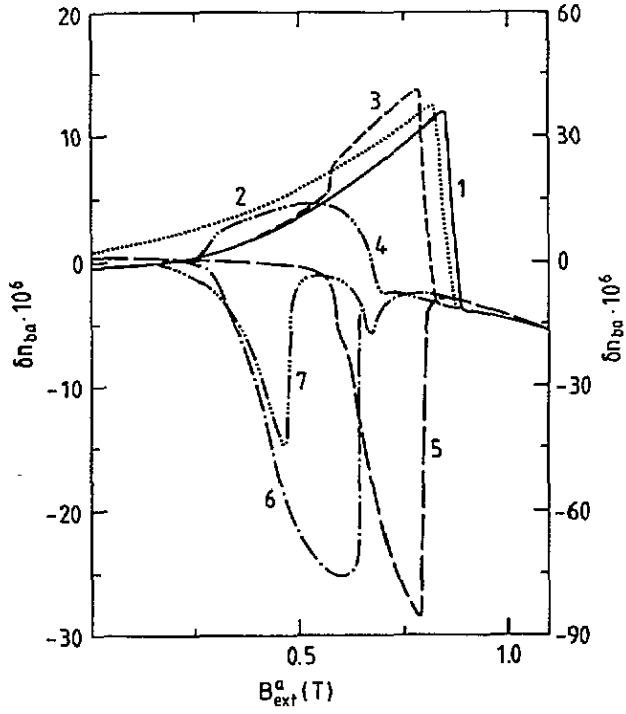

Figure 4. The *ba* birefringence measured at different temperatures and wavelengths as a function of the field strength along *a*: 1 and 2, $T = 1.42$ K, $\lambda = 633$ nm; 3, $T = 1.7$ K, $\lambda = 633$ nm; 4, $T = 2.0$ K, $\lambda = 633$ nm; 5, $T = 1.7$ K, $\lambda = 436$ nm; 6 and 7, $T = 2.0$ K, $\lambda = 436$ nm; 2 and 7 for decreasing, all other curves for increasing field; curves 1 to 4 left-hand scale, curves 5 to 7 right-hand scale.

$T_b^c = 1.90 \pm 0.03$ K and $B_b^c = 0.375 \pm 0.012$ T, as well (see for example Üffinger and Kasten 1985).

In the phase diagram with fields along x (figure 6), only the results of the present paper are exploited. The values of the temperature or the field strength at the phase transition were taken from the inflection points of the respective curves. When hysteresis is observed, the points determined for up and down sweeps are connected with horizontal or vertical bars. Here again, the agreement with the results of paper I and of Becker *et al* (1985) is fully satisfactory. In this field direction the two antiferromagnetic phases AF*xc* and AF*yc* with canted moments and monoclinic symmetry (where y or x, respectively, is the monoclinic axis) are clearly differentiated. But the spin-flop phase SF does not appear. The AF*xc*–AF*yc* transitions that were found in the field sweeps after premagnetizing the crystal in a field exceeding 0.72 T are not included in this figure. Thus, the region of the AF*yc* phase, as it is indicated in the figure, is valid only for a crystal that after cooling has not been in the PMo phase. The 'bicritical point', $T_b^x \simeq 2.01$ K and $B_b^x \simeq 0.5$ T, and the critical field (extrapolated to $T = 0$), $B_{c1}^x \simeq 0.74$ T, remain inaccurate. The AF*yc*–AF*xc* and AF*yc*/AF*xc*–PMo phase boundaries seem to be of first order.

The phase diagram with fields along *a* (figure 7) includes the results of the magnetic measurements of paper I (open symbols) and those of the birefringence measurements of the present paper (closed symbols, crosses or bars). Shifts of

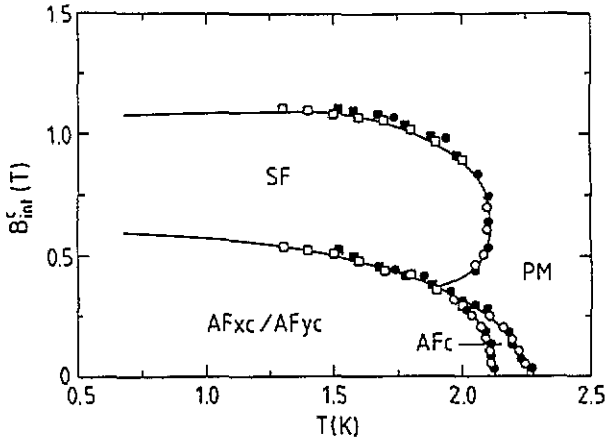

Figure 5. Experimental phase diagram of $TbPO_4$ with B_{int} along c, derived from magnetization (paper I, open symbols) and from Faraday rotation measurements (paper II, closed symbols). Demagnetization effects were taken into account, circles from temperature, squares from field sweeps. Full curves: average of the points measured by Üffinger and Kasten (1985). In papers I and II, the phases AFxc/AFyc and AFc are marked as AF′ and AF, respectively.

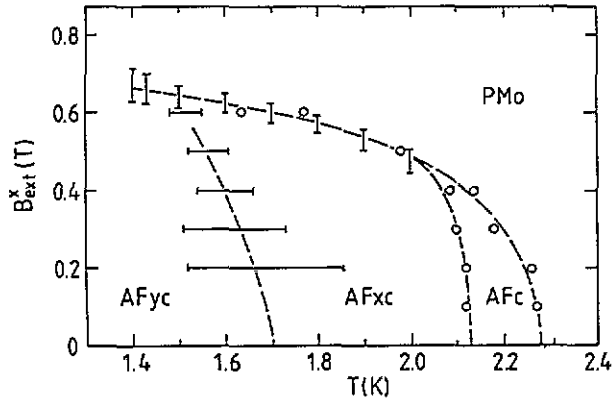

Figure 6. Experimental phase diagram of $TbPO_4$ with B_{ext} along x, derived from birefringence measurements (this paper, $N_x \simeq 0.36$). Demagnetization effects were not taken into account; the bars indicate the ranges of hysteresis; circles and horizontal bars from temperature, vertical bars from field sweeps. The broken curves are only guides to the eye.

the boundaries due to the different demagnetizing factors are unimportant since the magnetization itself is very small. Three phases, known from the other field directions, are clearly determined. These are the paramagnetic phase PM or PMo, respectively (saturated paramagnet with tetragonal or orthorhombic symmetry), the simple antiferromagnetic phase AFc and the antiferromagnetic phase AFxc or AFyc (which cannot be distinguished in this orientation). The AFc–PM phase boundary is obviously not perceptible in birefringence measurements. Whether the points indicated by crosses and those indicated by the horizontal bars (see section 3.2) represent phase transitions cannot be decided with certainty. Such an interpretation is, however, supported by the results of the calculations (see section 4). Consequently,

the phases PM and PMo are differentiated here already. The critical field (extrapolated to $T = 0$) is $B^a_{C1} \simeq 1.0$ T.

4. Model calculations and comparison with experiment

4.1. Mean-field approximation

The lowest crystal-field components of the Tb^{3+} ion in $TbPO_4$ at temperatures above 2.3 K are a doublet and three singlets. Their energies, numbering, symmetry types and the corresponding eigenfunctions are given in table 1 (after Böhm *et al* 1984). The singlets are composed of either symmetric or antisymmetric combinations of the pure $|M\rangle$ states of the ground term $^7F_6$, i.e. $|M\rangle_s = (|M\rangle + |-M\rangle)/\sqrt{2}$ or $|M\rangle_a = (|M\rangle - |-M\rangle)/\sqrt{2}$. These components form a group of states lying close to each other and separated from the others by a relatively large energy gap (of about 60 cm^{-1}). Therefore, the single-ion properties of Tb^{3+} will be described in a pseudo-spin formalism within a five-level system adapted to the tetragonal symmetry of the not magnetically ordered crystal.

Table 1. Lowest crystal-field components of Tb^{3+} in $TbPO_4$ (after Böhm *et al* 1984).

Energy (cm^{-1})	Numbering	Symmetry type	Eigenfunction
0.0	1, 2	Γ_5	$0.90\|\pm 5\rangle + 0.38\|\pm 1\rangle + 0.21\|\mp 3\rangle$
2.5	3	Γ_3	$0.93\|6\rangle_s + 0.36\|2\rangle_s$
9.5	4	Γ_4	$0.99\|6\rangle_a + 0.13\|2\rangle_a$
20.7	5	Γ_1	$0.83\|4\rangle_s + 0.56\|0\rangle$

Although some of the experimental facts observed below T_{N2} seem to be consistent with merely an orthorhombic Γ_3^+ distortion, the neutron diffraction experiments (Nägele *et al* 1980) have established a two-sublattice antiferromagnetic ordering with the moments canted off the c axis, which implies monoclinic symmetry. Nevertheless, in the calculations performed up to now only quadrupolar interactions corresponding to an orthorhombic distortion were introduced and the problem was restricted to the xz plane (Sivardière 1973, Kasten and Üffinger 1985, Bluck and Kahle 1988). These limitations will be removed now. A monoclinic Γ_5^+ distortion is additionally taken into account, the interactions according to the Γ_3^+ and Γ_5^+ distortions are considered in their full effectiveness and the restriction to the xz plane is eliminated by giving x and y equal status. Thus the problem is widened to a really three-dimensional one. Two sublattices (SL) are regarded to include magnetic ordering.

Within the approximation of linear coupling (Elliott *et al* 1972, Gehring and Gehring 1975), the mean-field Hamiltonian for an ion of SL 1 is given by

$$\begin{aligned} H = \Delta &- \beta_z\langle\sigma_2^z\rangle\sigma^z - \beta_x(\langle\sigma_2^x\rangle\sigma^x + \langle\sigma_2^y\rangle\sigma^y) - \alpha_z\langle\sigma_1^z\rangle\sigma^z - \alpha_x(\langle\sigma_1^x\rangle\sigma^x + \langle\sigma_1^y\rangle\sigma^y) \\ &- \tfrac{1}{2}\lambda_P(\langle P_1\rangle + \langle P_2\rangle)P - \tfrac{1}{2}\lambda_Q(\langle Q_1^x\rangle + \langle Q_2^x\rangle)Q^x \\ &- \tfrac{1}{2}\lambda_Q(\langle Q_1^y\rangle + \langle Q_2^y\rangle)Q^y - g_L\mu_B B_{ext}\sigma. \end{aligned} \tag{1}$$

For SL 2, the indices 1 and 2 have to be interchanged. In (1) Δ (contribution of crystal field), σ^z, σ^x and σ^y (magnetic interactions along z, x and y), P, Q^x and Q^y

(distortions of orthorhombic Γ_3^+ and monoclinic Γ_{5x}^+ and Γ_{5y}^+ symmetry, respectively) are 5×5 matrices. The coupling constants λ_P and λ_Q include Jahn–Teller coupling via exchange of phonons and coupling to uniform strain. $g_L = 1.5$ is the Landé factor. The other symbols have their usual meanings.

The non-zero matrix elements of the first four operators are (Kasten and Üffinger (1985), indices i, j = numbering of the components according to table 1): $\Delta_{33} = 3.6$ K, $\Delta_{44} = 13.7$ K, $\Delta_{55} = 29.8$ K, $\sigma_{11}^z = -\sigma_{22}^z = 4.06$, $\sigma_{34}^z = \sigma_{43}^z = 5.62$, $\sigma_{13}^x = \sigma_{31}^x = \sigma_{23}^x = \sigma_{32}^x = 1.49$, $\sigma_{14}^x = \sigma_{41}^x = -\sigma_{24}^x = -\sigma_{42}^x = 1.14$, $\sigma_{15}^x = \sigma_{51}^x = \sigma_{25}^x = \sigma_{52}^x = 2.26$, $\sigma_{13}^y = -\sigma_{31}^y = -\sigma_{23}^y = \sigma_{32}^y = \mathrm{i}1.49$, $\sigma_{14}^y = -\sigma_{41}^y = \sigma_{24}^y = -\sigma_{42}^y = \mathrm{i}1.14$, $-\sigma_{15}^y = \sigma_{51}^y = \sigma_{25}^y = -\sigma_{52}^y = \mathrm{i}2.26$. Symmetry and group theoretical arguments lead to the conclusion that, within the five-level system, two coupling constants are necessary to describe the coupling to the Γ_3^+ distortion and three constants to include the coupling to the Γ_5^+ distortion. Choosing the tensor operators appropriately and putting arbitrarily $\lambda_P = \lambda_Q = 1$ K, the coupling constants will be equal to the matrix elements of P and Q. These are: $P_{12} = P_{21} = pa$, $P_{35} = P_{53} = pb$, $Q_{13}^x = Q_{31}^x = -Q_{23}^x = -Q_{32}^x = qa$, $Q_{14}^x = Q_{41}^x = Q_{24}^x = Q_{42}^x = qb$, $Q_{15}^x = Q_{51}^x = -Q_{25}^x = -Q_{52}^x = qc$, $Q_{13}^y = -Q_{31}^y = Q_{23}^y = -Q_{32}^y = \mathrm{i}qa$, $Q_{14}^y = -Q_{41}^y = -Q_{24}^y = Q_{42}^y = \mathrm{i}qb$, $-Q_{15}^y = Q_{51}^y = -Q_{25}^y = Q_{52}^y = \mathrm{i}qc$. Thus, the constants $pa\lambda_P$, $pb\lambda_P$, $qa\lambda_Q$, $qb\lambda_Q$ and $qc\lambda_Q$ as well as β_z, β_x, α_z and α_x are the parameters that have to be determined by fitting the quantities (to be calculated by using equation (1)) to the experimental findings.

To get the thermal expectation values of the operators appearing in (1), coupled implicit equations for $\langle \sigma_{1,2}^{z,x,y} \rangle$, $\langle P_{1,2} \rangle$ and $\langle Q_{1,2}^{x,y} \rangle$ have to be solved iteratively. Since $TbPO_4$ experiences phase transitions of first order (which is revealed from the calculations as well) the equations have to be handled with different starting values. The thermodynamically most favourable solution is found by minimizing the free enthalpy of the two-SL system. Variation of the values of the constants leads finally to the optimum set of parameters.

The magnetic coupling constants for the c direction are established by the transition temperature T_{N1}, supposing, apart from the (calculable) dipole interactions, only nearest-neighbour exchange. Thus one gets $\beta_z = -0.16$ K (antiferromagnetic) and $\alpha_z = +0.02$ K. An attempt to use only the operator P or Q failed. It is not possible to obtain simultaneously low transition temperatures and the fact that the canted antiferromagnet AFxc in fields along x has sufficiently low susceptibility and is more favourable than AFyc. Thus it turns out that all interactions have to be taken into account. The coupling constants (including, to a certain extent, the nearest-neighbour exchange, too) are varied in order to reproduce, as satisfactorily as possible, the transition temperatures, the critical fields and the correct succession of the different types of phases. The optimal values of the parameters found in the fitting procedure are given in table 2. With these, the agreement between calculations and experimental findings is surprisingly good. It might, nevertheless, be possible to improve the results even more by expanding computer effort.

4.2. Phase diagram

4.2.1. Field in c direction. The phase diagram for fields along c, calculated for a crystal or a domain of the crystal with trend towards distortion in x direction, is reproduced in figure 8. For a crystal or domain with trend towards distortion in y direction AFxc and PMxc have to be replaced by AFyc and PMyc respectively. Comparing the diagram with the experimental one (see figure 5), a great accordance

Table 2. Parameter values found by fitting the Hamiltonian (1) to the experimental results.

$\beta_x = -0.17$ K	$pa\lambda_P = 1.07$ K
$\alpha_x = +0.02$ K	$pb\lambda_P = 3.9$ K
$\beta_x = -0.15$ K	$qa\lambda_Q = 0.87$ K
$\alpha_x = +0.05$ K	$qb\lambda_Q = 1.0$ K
	$qc\lambda_Q = 0.69$ K

is discernible. With the exception of PMxc (paramagnet, monoclinic crystal symmetry with y as monoclinic axis) all phases are essentially in agreement with experiment. The transition temperatures T_{N1} and T_{N2} and the critical fields B^c_{C1} ($T = 0$) and B^c_{C2} ($T = 0$) for the AFxc–SF and SF–PMxc boundaries, respectively, are placed a little too high. Moreover, the surroundings of the bicritical point are not correctly reproduced. The AFxc–SF and AFxc–AFc phase boundaries are found to be of first order, consistent with the experimental findings. The canting angle of the moments off the c axis in the AFxc phase at $T = 0$ is calculated to be 24.8°, in relatively good agreement with neutron diffraction (Coing-Boyat *et al* (1975); at 1.5 K, 26° as upper limit, 19.4° as most probable value). The PMxc phase, which extends theoretically up to the critical field B^c_{C3} ($T = 0$) = 10.2 T, has not been found in experiment despite repeated attempts. On the contrary, the infrared spectra taken at 1.6 K showed that the monoclinic distortion observed at zero field was suppressed by a field of 2.5 T along c (Prinz and Lewis 1983). Additionally, the inclusion of the Γ_5^+ distortion has brought the improvement that the SF phase does not directly extend up to 9 T without any intervening phase transition, as has been found in former calculations (Kasten and Üffinger 1985).

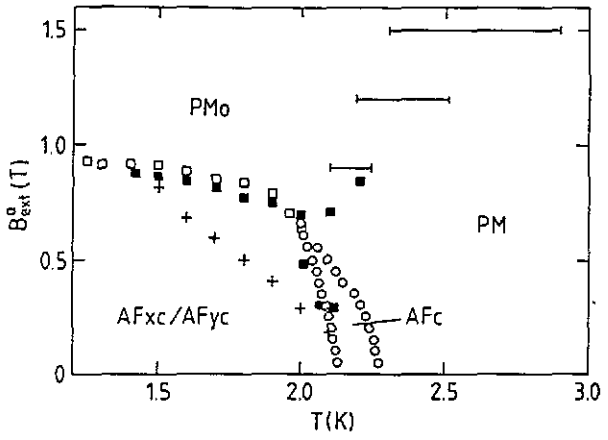

Figure 7. Experimental phase diagram of $TbPO_4$ with B_{ext} along a derived from magnetization (paper I, open symbols, $N_a \simeq 0.48$) and birefringence measurements (this paper, closed symbols, crosses or bars, $N_a \simeq 0.43$). Demagnetization effects were not taken into account; circles and horizontal bars from temperature, squares and crosses from field sweeps. For details concerning the crosses and bars see the text.

4.2.2. Field in x direction. The calculated phase diagram for fields along x (figure 9) is in excellent agreement with the experimental one (figure 6), again apart from the absolute values of the transition temperatures and critical fields. Whereas for fields

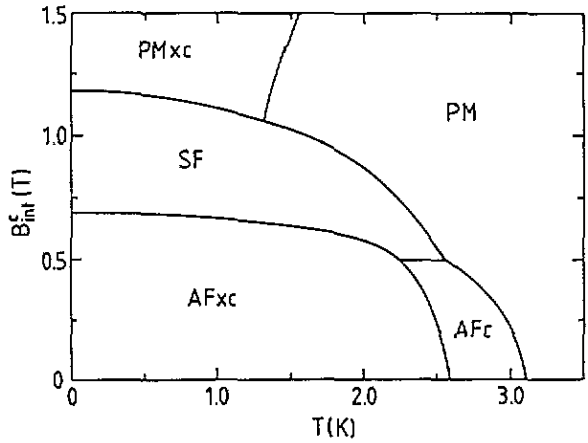

Figure 8. Calculated phase diagram with field along *c*. Coupling constants as in table 2.

along *c* the canting of the moments in the xc or the yc plane is energetically equal, this equivalence is removed for fields along x. The calculations show, in accordance with the experimental results, that the AFxc phase (xc canting) is favoured in the temperature range from 1.7 to 2.6 K and the AFyc phase (yc canting) at lower temperatures. All phase transitions, except those surrounding the AFc phase, are calculated to be of first order, which is not in contradiction to experiment. As a consequence of the field applied along x the PMo phase is Γ_3^+ distorted and the moments are tilted in x direction. The distortion is such that the expectation value $\langle P \rangle$ at $T = 3.5$ K and $B = 0.8$ T has about the same size as that at the AFxc–SF phase boundary at $T = 0$ for fields along *c*.

A surprising result is the phase that at low temperatures extends over a small wedge between AFyc and PMo. It has a strong Γ_3^+ distortion in x direction (about three times as high as the PMo phase in the vicinity). Experimental evidence might be the observation of a jump in the downward field sweep of the yx birefringence at 1.4 K at a field of 0.62 T; see curve 4 of figure 1. This jump can, however, be explained just as well as the PMo–AFyc phase transition that holds up to lower fields due to hysteresis. Thus lower temperatures are required to render possible clear statements.

The AFyc–AFxc phase boundary is identified by a large jump in the expectation value of the Γ_3^+ distortion operator $\langle P \rangle$. In the expectation value of the pseudo-spin $\langle \sigma^x \rangle$, on the contrary, there is no change at all for small fields B^x and only a very small but steady change for fields just below the PMo phase boundary. That will be the reason for not being able to prove this phase transition by magnetic investigations. One of the results of paper I was that, for low fields along x, the measured parallel ($\chi_{\parallel x}$) and perpendicular ($\chi_{\perp x}$) susceptibilities are equal even for a single-domain crystal. This is consistent with the calculated $\langle \sigma^x \rangle$, which, at low fields, is equal in the phases AFyc (where it corresponds to $\chi_{\perp x}$) and AFxc (where it corresponds to $\chi_{\parallel x}$).

4.2.3. Field in a direction. A magnetic field along *a* makes an angle of 45° with respect to the distortion directions x and y. Hence these two directions are equivalent, and the crystal will be divided into domains with x or y distortion, respectively. The calculated phase diagram of a domain with trend towards distortion in x direction is displayed in figure 10. That of a domain with trend towards distortion in y direction

is analogous with AF*xc* replaced by AF*yc*. It turns out that a further antiferromagnetic phase AF*bc* exists for this field direction besides the AF*c* and AF*xc* phases. This additional phase has a Γ_{5b}^{+} but no Γ_{3}^{+} distortion (a axis as monoclinic axis). The Γ_{5b}^{+} distortion impedes a tilting of the magnetic moments off the c axis in b direction (away from their antiparallel orientation along $\pm c$), but lightens a tilting in a direction. Consequently, this phase with Γ_{5b}^{+} distortion is thermodynamically more favourable than one with the orthogonal Γ_{5a}^{+} distortion.

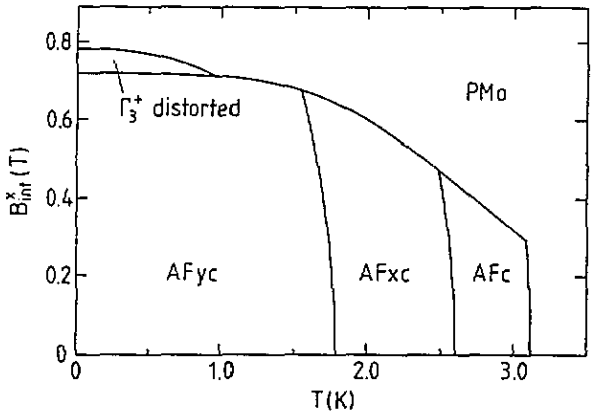

Figure 9. Calculated phase diagram with field along x. Coupling constants as in table 2.

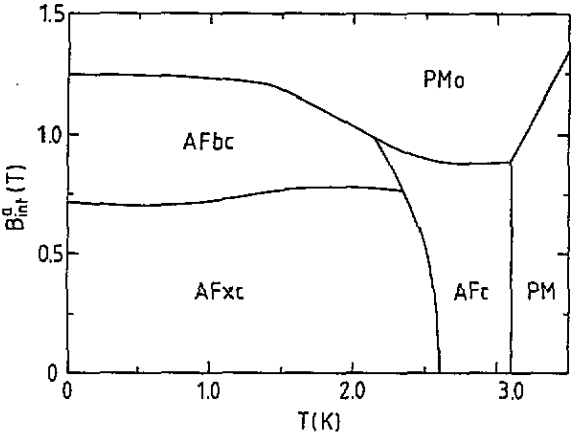

Figure 10. Calculated phase diagram with field along a. Coupling constants as in table 2.

For fields above about 1.25 T, the crystal turns over, in a first-order phase transition, into a paramagnetic phase PMo with relatively large Γ_{3}^{+} distortion. The moments are oriented almost within the xc plane but with a small tilting into the a direction. Since the field produces an additional Γ_{4}^{+} distortion, the symmetry is, strictly speaking, monoclinic. According to the calculations, this phase extends up to 18.2 T at $T = 0$. It is separated from the undistorted PM phase by a boundary that shows an almost linear relation between the increase in field and temperature.

The agreement between calculated and measured (figure 7) phase diagrams is not as satisfactory as for the other two field directions. The phases AF*xc*, AF*c* and PM (or PMo) have been detected in experiment, albeit not perfectly in the same temperature and field region. But the phases AF*bc* and PMo (or PM) could not be identified directly. Measurements of the *ba* birefringence (see section 3.2) gave indications though that the PMo–PM (bars in figure 7) and AF*xc*–AF*bc* phase boundaries (crosses) might have been found, but other explanations cannot be denied. Support for the existence of the PMo phase follows, however, from the infrared spectra taken at 4.2 K by Prinz and Lewis (1983). Their analysis revealed a monoclinic distortion in fields along a of growing size, starting at about 2.0 T (measured up to 10 T). This distortion was found to be different from that of the AF*xc*/AF*yc* phases. At 4.2 K, the PM–PMo phase boundary lies, according to our calculations, just at 2.0 T.

4.3. Other measured quantities

The capability of the mean-field approach is enhanced by the fact that the temperature and field dependences of other physical properties can be calculated in very good agreement with the experimental results. Two examples will be dealt with in the following.

In the first one, the calculated temperature dependence of the expectation value of the Γ_3^+ distortion operator $\langle P \rangle$ (curve 1 of figure 11) is contrasted with the measured temperature sweep of the yx birefringence (curve 2). Here the temperature axis for the curve of $\langle P \rangle$ is linearly compressed (by a factor of 0.8) to bring the calculated and the measured (2.10 K) temperature of the AF*xc*–AF*c* phase transition into coincidence. Although the distortion of the Γ_5^+ type was disregarded, the agreement is surprisingly good. Obviously, the proportionality between distortion and birefringence is valid to a large extent even in such a complex system. The curve of $\langle P \rangle$ shows first a large jump from negative to positive values at the AF*yc*–AF*xc* boundary, then a decrease in the AF*xc* phase, an increase in the AF*c* phase with a small jump at the PM boundary and finally a decrease in the PM phase. As expected, it follows that even the AF*c* and PM phases with originally tetragonal symmetry get a Γ_3^+ distortion due to magnetostriction in a field along x.

The second example concerns the magnetizations for fields along c, x and a or rather the proportional quantities, namely the expectation values of the pseudo-spin operator, $\langle \sigma^c \rangle$, $\langle \sigma^x \rangle$ or $\langle \sigma^a \rangle$, respectively. Figure 12 shows the results of the calculation using the parameters of table 2. The overall agreement with the measurements (see figure 2 of paper I) is unexpectedly good, in spite of some deviations in the absolute values and in the gradient of the curves. The finite slopes (instead of jumps) at the AF*xc*–SF or AF*xc*–PMo boundaries are caused by the calculation in steps. In particular, the figure confirms the experimental result that the magnetizations along x and a are almost equal for fields up to about 0.6 T. In consequence, one has to conclude that the expectation value $\langle \sigma \rangle$ in the field direction (at moderate fields) for a single-domain crystal is not only equal for fields in x or in y direction (as explained at the end of section 4.2.2), but equal even for all field directions in the basal plane. This is really surprising for a crystal having monoclinic symmetry.

Finally an attempt will be made to explain the measured field dependence of the magnetization for fields along x. Here a vertical jump is observed at the AF*yc*–PMo boundary already without demagnetization and an overhanging to the left after demagnetization (see section 3.1 of paper I). The particularity for this field direction

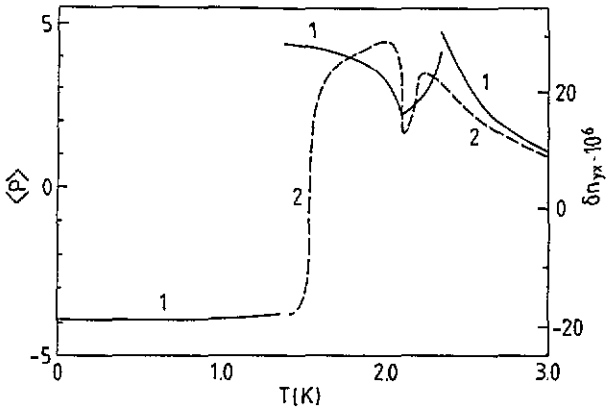

Figure 11. Comparison of the calculated expectation value of the Γ_3^+ distortion operator $\langle P \rangle$ (curve 1, left-hand scale) with the measured yx birefringence (curve 2, right-hand scale, $\lambda = 436$ nm, decreasing T) as a function of temperature, both at a field $B^x = 0.3$ T. The temperature axis for $\langle P \rangle$ is compressed by a factor of 0.8 to bring the transition temperature $T_{N2} = 2.10$ K into line.

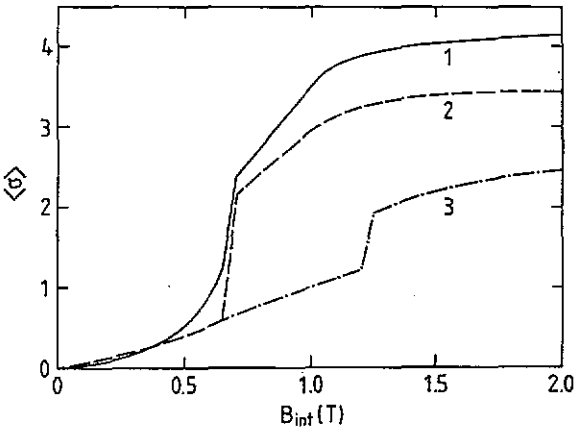

Figure 12. Expectation value of the pseudo-spin in field direction, $\langle \sigma^c \rangle$, $\langle \sigma^x \rangle$ or $\langle \sigma^a \rangle$, respectively, for fields along c (curve 1), along x (curve 2) and along a (curve 3) at 1.4 K, calculated in steps of 50 mT.

is that the crystal is single-domain in the AFyc as well as in the PMo phase, whereas, however, the Γ_3^+ distortions in the two phases are orthogonal to one another. The redistortion of the crystal in crossing the phase boundary requires first the creation of centres with the new distortion direction. Consequently, the phase transition is determined not only by a potential barrier but also by the conditions for the miscibility and consistency of the two phases. These requirements obviously lead to the consequence that the crystal is not in the equilibrium state that is required by the field including demagnetization, so that the overhanging curve results. For the other two field directions (along c and a) the crystal is multi-domain in at least one of the adjacent phases (for example in AFxc/AFyc). This has the consequence that one of the domain types can act as centres for starting the redistortion of the crystal. Hence, no exceptional features exist at these phase transitions.

5. Conclusions

Linear optical birefringence has proved to be a very successful tool for the investigation of the low-temperature properties of $TbPO_4$. Although its birefringence is small in comparison with that of related Jahn–Teller-active compounds, the anomalies and changes at phase transitions were clearly determinable. For fields along x a new combined structural and magnetic transition was found with certainty that separates two areas having orthogonal distortions and antiferromagnetic structures with the moments canted off the c axis. The canting occurs within the plane perpendicular to the field direction for the lower-temperature phase AFyc (which is spin-flop like) and it occurs into the field direction for the higher-temperature phase AFxc (which is spin-flip like). This phase boundary is not discernible in magnetic investigations. Other additional anomalies could not definitely be identified as phase transitions.

The results of the birefringence measurements and those of the magnetization (paper I) and Faraday rotation (paper II) led to a precise determination of the phase diagram of this substance for three principal field directions.

Calculations in mean-field approximation within the basis of the five lowest Tb^{3+} states, including magnetic interactions and crystal distortions, gave an important contribution to the understanding of the properties of the diverse phases. Many of the physical quantities (which were not used in the fitting process for the interaction constants) could be reproduced nearly quantitatively.

In spite of the considerable improvement in the understanding of the low-temperature behaviour of $TbPO_4$, achieved by this series of investigations, several problems remain open. Some examples of this are: the explanation of the hysteresis observed at many of the phase transitions; the elucidation of the overhanging demagnetized curve of the magnetization for fields along x; the investigation of the properties at higher fields (above about 2 T), especially along a; and those at lower temperatures (below 1.4 K), especially for fields along x. Among others, single-crystal neutron diffraction measurements seem promising to corroborate the magnetic structures of some of the phases that, up to now, result from calculations only.

References

Anderer C, Hess G and Kahle H G 1993 *J. Phys.: Condens. Matter* **5** 945–54
Becker P J, Kahle H G and Keller E 1985 *Phys. Status Solidi* b **130** 191–6
Bluck S and Kahle H G 1988 *J. Phys. C: Solid State Phys.* **21** 5193–208
Böhm W, Kahle H G and Wüchner W 1984 *Phys. Status Solidi* b **126** 381–92
Coing-Boyat J, Sayetat F and Apostolov A 1975 *J. Physique* **36** 1165–74
Elliott R J, Harley R T, Hayes W and Smith S R P 1972 *Proc. R. Soc.* A **328** 217–66
Gehring G A and Gehring K A 1975 *Rep. Prog. Phys.* **38** 1–89
Hess G 1990 *J. Phys.: Condens. Matter* **2** 1097–112
Hintzmann W and Müller-Vogt G 1969 *J. Crystal Growth* **5** 274–8
Kahle H G and Müller A U 1992 *J. Magn. Magn. Mater.* **104–7** 1187–8
Kasten A and Üffinger G 1985 *Phys. Status Solidi* b **128** 525–35
Mensinger H, Jakelski J, Kahle H G, Kasten A and Paul W 1993 *J. Phys.: Condens. Matter* **5** 935–44
Nägele W, Hohlwein D and Domann G 1980 *Z. Phys.* B **39** 305–10
Prinz G A and Lewis J F L 1983 *J. Magn. Magn. Mater.* **39** 285–9
Rado G T, Ferrari J M and Maisch W G 1984 *Phys. Rev.* B **29** 4041–8
Sivardière J 1973 *Phys. Rev.* B **8** 2004–15
Üffinger G and Kasten A 1985 *Phys. Status Solidi* b **128** 201–7